INL/RPT-22-70360-Revision-0

Laboratory and In-Pile Testing of a Fiber-optic Pressure Sensor

November 2022

Austin D Fleming, Ashley A Lambson

Changing the World's Energy Future

INL is a U.S. Department of Energy National Laboratory operated by Battelle Energy Alliance, LLC

INL/RPT-22-70360-Revision-0

Laboratory and In-Pile Testing of a Fiber-optic Pressure Sensor

Austin D Fleming, Ashley A Lambson

November 2022

Idaho National Laboratory
Idaho Falls, Idaho 83415

http://www.inl.gov

Prepared for the
U.S. Department of Energy
Under DOE Idaho Operations Office
Contract DE-AC07-05ID14517

INL/RPT-22-70360

Laboratory and In-Pile Testing of a Fiber Optic Pressure Sensor

November 2022

Summary Report – M2CT-23IN0702025

Austin Fleming and Ashley Lambson
Idaho National Laboratory

Idaho National Laboratory

INL is a U.S. Department of Energy National Laboratory
operated by Battelle Energy Alliance, LLC

INL/RPT-22-70360

Laboratory and In-Pile Testing of a Fiber Optic Pressure Sensor

Summary Report – M2CT-23IN0702025

Austin Fleming and Ashley Lambson

November 2022

Idaho National Laboratory
Idaho Falls, Idaho 83415

http://www.inl.gov

Prepared for the
U.S. Department of Energy
Office of Nuclear Energy
Under DOE Idaho Operations Office
Contract DE-AC07-05ID14517

Page intentionally left blank

SUMMARY

In this report, the development, testing, and deployment of a fiber-optic-based extrinsic Fabry-Perot pressure sensor is discussed. Details on the design and fabrication procedure are discussed, and the methodology for making design decisions is provided. The results of the laboratory-based testing and calibration are provided, along with preliminary data from in-pile testing in the Transient Reactor Test Facility.

Page intentionally left blank

ACKNOWLEDGEMENTS

This work was supported through the Nuclear Energy Enabling Technology (NEET) Advanced Sensor and Instrumentation (ASI) Program and Nuclear Science User Facilities (NSUF), under Department of Energy (DOE) Idaho Operations Office contract no. DE-AC07-05ID14517.

Page intentionally left blank

CONTENTS

FIGURES

ACRONYMS

HERA High Burnup Experiments in Reactivity Initiated Accidents

Page intentionally left blank

Laboratory and In-Pile Testing of a Fiber Optic Pressure Sensor

1. INTRODUCTION

In-pile instrumentation affords various types of measurements for conducting research, development, and qualification on nuclear fuels and materials—and in some cases, for creating operation requirements for nuclear reactors. Depending on the objective, these sensors may be located in high-radiation (neutron and gamma), high-temperature, high-pressure, and/or corrosive environments. While it is impossible to design a sensor that is suited to all manner of possible conditions, a few are of particularly high interest to designers of various reactor technologies, including those related to pressurized-water reactors, sodium-cooled fast reactors, high-temperature gas reactors, and molten-salt reactors. These wide-ranging reactor technologies entail vastly different measurement requirements and irradiation conditions.

No commercially available sensor exists that can meet virtually all in-pile measurement needs. This is primarily due to the low volume and high cost of the development and testing required, and is ultimately why the Advanced Sensors and Instrumentation program developed the pressure sensor discussed in this report, which covers the design considerations involved and provides an overall discussion of the sensor design, fabrication, and calibration processes. It also covers sensor testing—both in a laboratory and an in-pile setting. Finally, a summary is provided, as well as the maturation path forward for this sensor.

2. SENSOR DESIGN

Due to the time, cost, and effort required to develop and qualify a sensor for in-pile applications, it is desirable to satisfy as many needs as possible via a single sensor. Therefore, the pressure sensor detailed in this report was optimized to withstand the highest operating temperature possible, was constructed out of materials suited to many types of extreme environments, and was made to be easily reconfigurable for different pressure ranges. Several aspects of this sensor are still in development or are undergoing design revisions to improve performance. The following subsections discuss the overall sensor design and measurement technique, followed by the material selections, geometric constraints, and fabrication process.

2.1 Extrinsic Fiber Optic Fabry-Perot Design

In 2018, a plan was established to develop a fiber optic pressure sensor [1]. In creating that plan, it was determined that an extrinsic Fabry-Perot pressure sensor would best suit the needs of nuclear energy applications. Extrinsic Fabry-Perot sensors utilize the interference of light between two reflecting surfaces. In this design, the ends of the fiber and diaphragm serve as these reflective surfaces. This design minimizes the impact of radiation effects, since it is based on an interferometric measurement instead of a magnitude measurement. The diaphragm deflects (toward the fiber) due to external pressure on the sensor. The diaphragm's thickness and diameter are the main parameters used to modify the pressure range of the sensor. The displacement at the center of a diaphragm with fixed edges is given by:

$$y_o = \frac{3(1-\mu^2)Pa^4}{16Eh^3} \tag{1}$$

where P is pressure, a is the radius of the diaphragm, E is the modulus of elasticity, h is the thickness of the diaphragm, and μ is Poisson's ratio. This simple equation shows a linear dependence between pressure and displacement—as is ideal for a sensor. Additional details on material selection and stress limitations for diaphragms are found in our previous report [2].

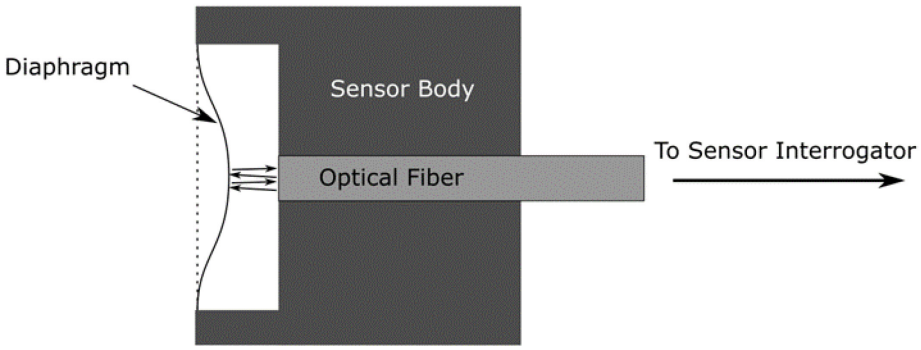

Figure 1. Sensor diagram showing the overall working concept for an extrinsic fiber optic Fabry-Perot pressure sensor.

In the present work, a Micron Optics si155 was used to interrogate the sensor, whose wavelength bandwidth ranges from 1480 to 1620 nm, thus capturing many periods of constructive and destructive interference. An example of an interference spectrum is given in Figure 1. After recording the spectra, the data are processed by first identifying the locations of all the peaks in the spectra. This is accomplished by using a Python script to conduct a quick analysis to serve as the basis for initial guesses as to the peak locations. Once these initial guesses are established, a parabola is fit to the data point near the initial guesses to further refine the identification of the peaks. The spacing between two adjacent peaks in the spectrum (where constructive interference occurs) is used to determine the cavity length via:

$$L = \frac{\lambda_1 \lambda_2}{2n(\lambda_2 - \lambda_1)} \tag{2}$$

where λ_1 and λ_2 are the wavelengths of adjacent peaks, n is the refractive index of the gas inside the sensor, and L is the cavity length.

After all the peak wavelengths are identified, they are used with (2 to calculate the cavity length based on all adjacent peak wavelengths. This data analysis is required for each pressure measurement. The si155 full spectrum recording is limited to 10 Hz, which does not meet the measurement requirements for certain high-speed phenomena. However, collecting data at 10 Hz over extended periods of time can amount to significant quantities of data that must be processed. Work to optimize this data acquisition/processing approach remains ongoing to improve both accuracy and the time required to process the data.

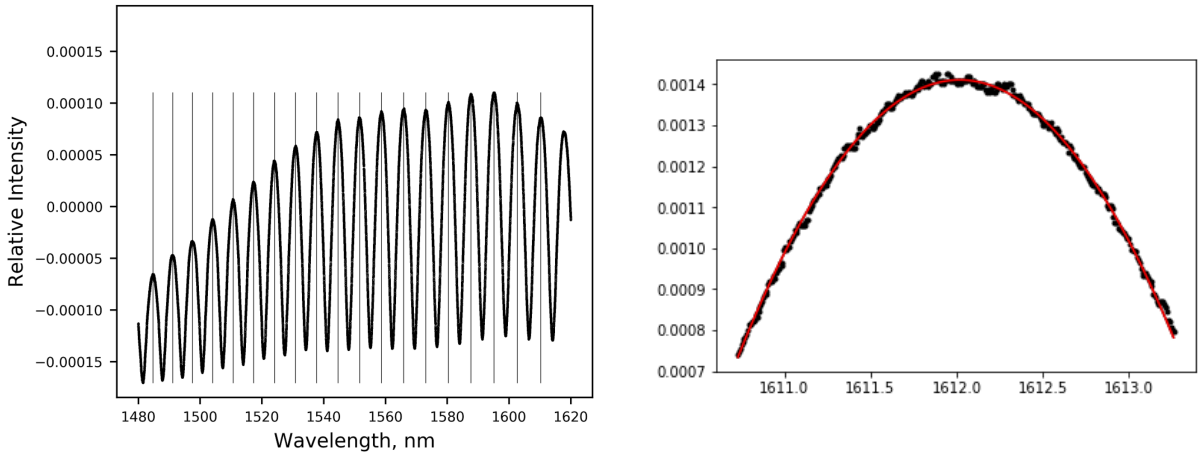

a b

Figure 2. (a) A measured spectrum from a pressure sensor, with the peak locations identified. (b) Example of a parabola (red) being fit to the data points near a peak in order to further refine the peak identification.

2.2 Material Selection

Silica-based optical fibers are incompatible with many of the environments of interest. The environments generated within pressurized-water reactors represent a key type of environment with which silica is not directly compatible, due to the interaction between the water and the silica. This precludes the use of the all-silica designs commonly found in the literature. Additionally, these all-silica designs are quite fragile, considering they will be required to operate in industrial environments. Stainless steels 304 and 316 provide some of the best compatibility with a variety of reactor designs. These austenitic alloys provide excellent corrosion resistance and strong high-temperature performance. While other materials have better mechanical properties for sensor performance, environmental compatibility takes priority. The pressure sensor discussed here was fabricated from both stainless steel 304 and 316, both of which offer very similar performance. These stainless steels were used for the ferrule, sensor body, diaphragm, protective tube, and lead-out capillary tube.

A single-mode optical fiber was used in the sensor. For higher radiation tolerance, a pure silica core with a F-doped cladding is recommended. For low-dose applications, the material composition of the glass is less important. For high-temperature applications, the fiber coating should be considered. The most common optical fiber coatings include: acrylate, polyimide, and metal (commonly aluminum, copper, and gold). From an optical perspective, the coating has no impact on the measurement, but strongly impacts the fabrication process and the ruggedness. The metal-coated fibers have the highest operating temperatures but require more complicated processes for fabricating connectors and removing the coatings for splicing activities. During development of this pressure sensor, polyimide-coated optical fiber was used because of its relatively high temperature rating (i.e., ~350°C), but we have since transitioned to using copper-coated optical fiber for the section near the sensor head in order to achieve higher temperature capabilities. We also transitioned to polyimide-coated fiber for the lead-out section of the sensor.

Ensuring that the fiber adheres to the ferrule in the sensor body is crucial to sensor performance. Low-viscosity epoxies that are standard for fiber optic applications work well for this sensor in low-temperature and low-radiation applications. However, in higher temperature/radiation environments, other adhesives must be used. These alternative adhesives must rigidly affix the fiber to the ferrule and create a hermetic seal between the two. The sensor can experience significant drift if the hermetic seal is not maintained, since the pressure on the internal side of the diaphragm is not held constant. The current

nominal design involves using an induction furnace to perform a braze weld between a copper-coated metal fiber and the ferrule, using zinc wire as a filler. The zinc enables the braze weld to be performed without damaging the fiber or its coating. This is because zinc has a relatively low melting point (i.e., 420°C), which also serves to strongly limit the high-temperature operation of this design. Ceramic adhesives are currently being tested for higher temperature operation. While the sensor is still under development, the adhesive is likely to be the limiting parameter in terms of the sensor's high-temperature rating.

2.3 Geometric Constraints

Size and shape are key limitations of commercially available pressure transducers. In irradiation experiments, the desired pressure measurement is often a very localized phenomenon of interest, so the measurement device must be located in that spot. One example is the plenum pressure inside a fuel rodlet. The internal pressures of the fuel rods increase as fission gas is released from the nuclear fuel into the plenum of the fuel rod. In this scenario, the pressure sensor must be encapsulated within the fuel rod, or at least connected to the outside of it. Many transient scenarios require a localized pressure measurement because reflecting and dissipating pressure waves can result in erroneous measurements when conducted remotely. For nearly all applications, the smallest size possible is preferable from a deployment standpoint. However, this must be balanced with sensor performance considerations.

2.4 Fabrication Procedure

The first step in the fabrication procedure is to weld the lead-out capillary tube to the fiber ferrule, then perform a helium leak check to ensure it is sealed. Next, an optical fiber is inserted through this assembly and adhered to the ferrule via either high-temperature epoxy, brazing compounds, or other high-temperature adhesives. The ferrule is then polished using standard fiber optic polishing equipment. The polished face forms the first reflective surface of the Fabry-Perot cavity. Meanwhile, the protective tube, diaphragm, and center sensor body are welded together in an inert atmosphere. The optical fiber is then connected to an interrogator, while the sensor body (with diaphragm and tube welded together) is installed to the ferrule. This allows the sensor to be read out so as to determine its cavity length. The sensor body can then be shortened to the desired cavity length by using facing equipment or abrasive materials. Measurement resolution is improved with shorter cavity lengths, but the diaphragm must not contact the fiber. During the final welding process, some relative motion can occur, and this should be accounted for in the fabrication process. Once the desired cavity length is achieved, the final weld is performed between the sensor body and the ferrule. Finally, the protective tube is cut to length, making the sensor ready for testing and calibration.

3. TESTING

The sensor has been tested in both a laboratory setting and in-pile. The two following subsections will discuss some of these results with an emphasis on the temperature effects on sensor performance. The temperature sensitivity calculated analytically is compared to experimental data. Some data from the first in-pile testing of the sensor is provided.

3.1 Laboratory Testing

This fiber optic pressure sensor was significantly tested in a laboratory setting that included a pressure-controlled environment inside a furnace to determine the cross sensitivity of the temperature effects on the pressure measurement. This system had a long section of uniform temperature in the center of the furnace, and a Fluke 700G08 monitored the system pressure. This setup was used to perform sensor testing and calibration prior to in-pile deployment of the sensor. After the sensor fabrication was complete, the diaphragm was preconditioned by pressurizing it to 110% of its maximum design pressure, then releasing the pressure 10 times. Following this, calibration of the sensor began by first taking a spectrum over the complete range of design pressures—starting at atmospheric pressure, ramping up to

maximum pressure, and then moving back down to atmospheric pressure. This process was conducted twice, meaning that four spectra were collected at any given pressure (two while the pressure was increasing, and two while it was decreasing). This provided some statistical information on sensor repeatability, and served to trace out two hysteresis loops.

An example of these calibration data is given in Figure 3. The cavity length was measured via the process described above, and the pressure was *known* from the reference pressure gauge. Due to limited control of the pressure regulator, the exact pressure was difficult to achieve at each step, resulting in some spread in the data along the x-axis (and the corresponding cavity length). The error bars are two standard deviations resulting from calculating the cavity lengths from all adjacent peak wavelengths. The excellent sensor linearity was the first thing observed from these data, and was an element of sensor performance that was both expected and desired in this case. Additionally, the hysteresis of the diaphragm was well within the measurement uncertainty introduced by the data reduction process. To improve sensor accuracy, better data reduction algorithms or increasing diaphragm displacement with pressure can be implemented (ideally both). The error bars are remarkably constant across the pressure range, indicating that the random uncertainty is a constant rather than a percentage of the measurement.

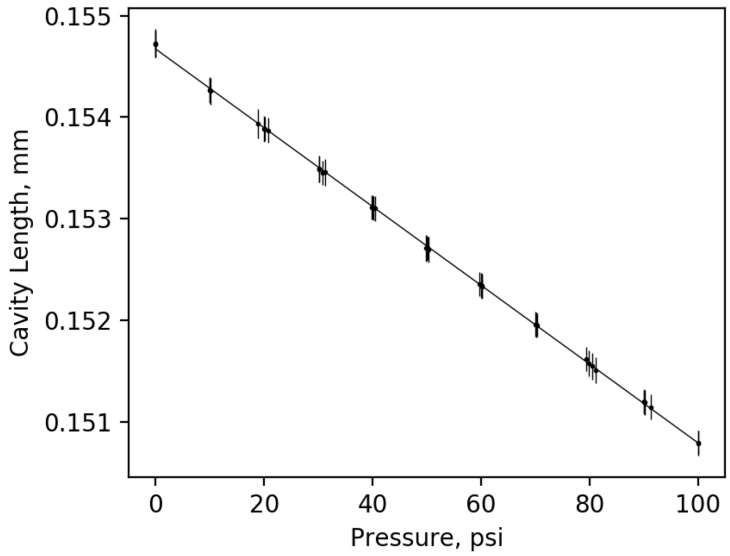

Figure 3. Calibration curve for a fiber optic pressure sensor, correlating the measured cavity length to a known pressure. The error bars are two standard deviations.

Sensor behavior at elevated temperatures is a key metric for sensor performance. Quantifying changes in sensitivity or other sources of induced error is necessary for sensor qualification. Three key phenomena related to changes in temperature have been identified that can impact the sensor performance. The first is the pressurization of the reference cavity internal to the sensor due to the ideal gas law. The second one is the thermal expansion of the sensor body. The third is due to the material property changes of the diaphragm with respect to temperature.

The reference cavity is the volume of space that is enclosed by the inside of the sensor body, ferrule, and diaphragm which is sealed with the final weld during fabrication. This weld is conducted in an argon filled glovebox which is maintained near atmospheric pressure. The temperature of the gas during the sealing process is elevated due to the welding process, but the exact temperature is unknown. The ideal gas law is given by

$$PV = nRT \tag{3}$$

where P is the pressure, V is the volume, n is the moles of gas, R is the universal gas constant, and T is the absolute temperature. Once the cavity is sealed, changes in volume are negligible and the moles of gas is a constant. The ideal gas law can then be used to write the pressure and temperature in the following form

$$\frac{P_1}{T_1} = \frac{nR}{V} = \frac{P_2}{T_2} \tag{4}$$

where the subscripts denote any two conditions. For subscript one, we can consider the state of the sensor at room temperature after the sensor is sealed, thereby T_1 is 20 C (293.15 K). P_1 is unknown, however, since it is sealed at atmospheric pressure at an elevated temperature we can conclude that at room temperature the pressure is less than that of atmospheric pressure ($P_1 \leq 14.7psi$). Rearranging equation (4) a simple relationship is found for the pressure in the reference cavity as a function of temperature.

$$P_2 = \frac{T_2}{T_1} P_1 \tag{5}$$

The pressure in equation (1) refers to the change in pressure across the diaphragm. Therefore, the pressure differential experienced by the diaphragm is the external pressure minus P_2. It should be noted that from equation (5) that the lower pressure P_1 the less impact temperature can have on sensor performance by increasing the reference volume pressure. This is a consideration for sensor construction, and provides a potential path for improving future sensor performance.

The thermal expansion of a material is defined by

$$\Delta L = L_0 \alpha \Delta T \tag{6}$$

where L_0 is the length of the material, α is the thermal expansion coefficient, and ΔT is the change in temperature the material experiences. For this consideration L_0 is the cavity length, which is the distance between the ferrule and the diaphragm, and the ΔT is the change in temperature measured from room temperature.

The modulus of elasticity of the diaphragm is also impacted by the temperature, which is strongly material dependent. For this work the temperature dependence of the modulus of elasticity was taken from the ASME boiler and pressure vessel code [3]. The provided value of modulus of elasticity is plotted in Figure 4, and a linear fit for the data from 20 C to 600 C is provided. This linear fit is later used for the analytic calculation of sensor performance at elevated temperatures.

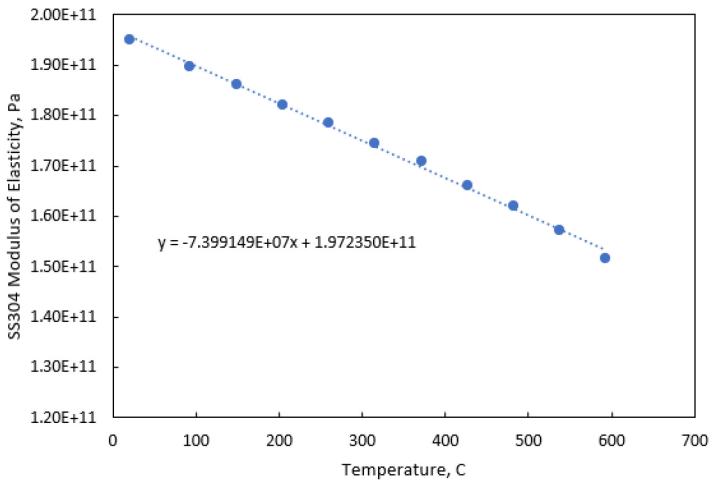

Figure 4. Temperature dependence of the modulus of elasticity for stainless steel 304 provided from the ASME Boiler and Pressure vessel code.

Combining these effects we can obtain the cavity length as

$$L(T,P) = L_0 + L_0\alpha(T - T_1) - \frac{3(1-\mu^2)\left(P - \frac{T}{T_1}P_1\right)a^4}{16Eh^3} \tag{7}$$

and the derivatives with respect to temperature as

$$\frac{\partial L}{\partial T} = L_0\alpha - \frac{3(1-\mu^2)a^4\frac{P_1}{T_1}}{16Eh^3} \tag{8}$$

and pressure as

$$\frac{\partial L}{\partial P} = -\frac{3(1-\mu^2)a^4}{16Eh^3}. \tag{9}$$

With these derivatives it can be observed that neither depend on temperature or pressure indicating the changes with respect to both should be linear. The only exception to this is the modulus of elasticity which has a small temperature dependence.

The temperature cross sensitivity of the sensor was tested experimentally using the calibration facility. The data from the cross-sensitivity testing of one sensor is presented in Figure 5. Using equation (7) the cavity length is calculated for a pressure range from 0 to 100 psig is provided in Figure 6 for three different temperatures. For this calculation the nominal cavity length is selected to be 70.8 μm for easy comparison to the experimental results in Figure 5.

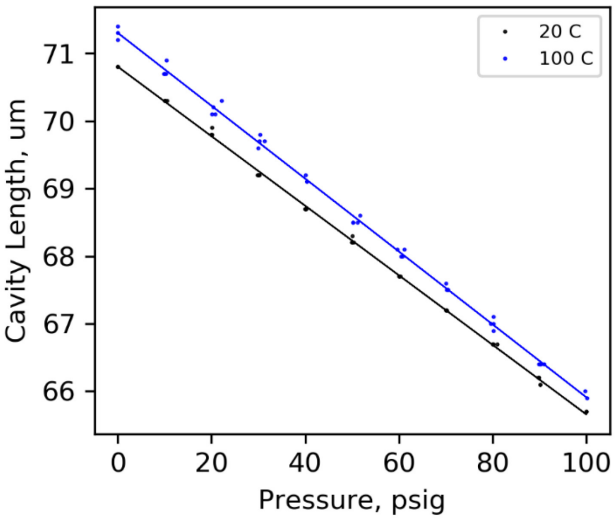

Figure 5. Measured sensor cavity length for pressures ranging from atmospheric to 100 psi for temperature of 20 C and 100 C.

The excellent agreement between the analytic prediction and experimental results is the first aspect that should be noted. The linear response is predicted by equation (7) is observed in all scenarios. The increased cavity length with respect to temperature is established by both thermal expansion and reference cavity pressurization. The different values in slope for each plot is a result of the temperature dependence on the modulus of elasticity of the diaphragm.

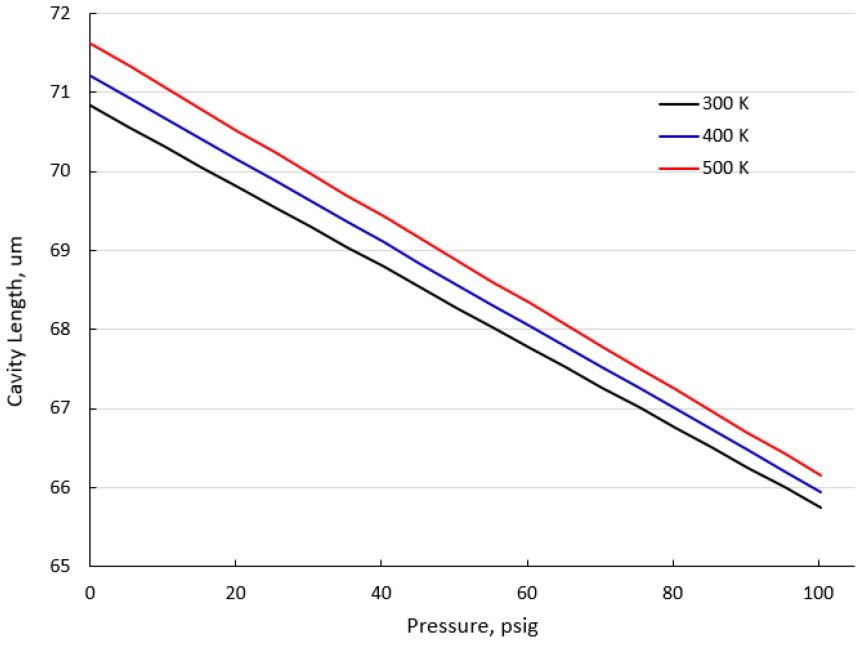

Figure 6. Calculated cavity length plotted over a range of pressures for three temperature ranges

3.2 In-Pile Testing

This sensor was incorporated into the High Burnup Experiments in Reactivity Initiated Accidents (HERA) experiment for measuring the capsule pressure during irradiation. In some of these HERA irradiation experiments, the capsule pressure only experiences a small increase in pressure from the elevated temperature of the capsule plenum. However, some experiments will experience boiling events that lead to a strong increase in pressure as a result of the vapor pressurizing the capsule. No other commercially available sensors could be accommodated to make this measurement, due to the temperature, irradiation, and size constraints involved. Thus, there is no reference temperature against which to compare the results. Additionally, the model for predicting the pressure increases has significant uncertainty bounds. Therefore, sensor performance is not being evaluated via a quantitative comparison to a known or controlled value. Rather these results are looking to observe the radiation hardness of the sensor, as well as whether it can survive the high-flux conditions observed in these experiments. The pressure measurements can also be interpreted for correctness based on the qualitative trends.

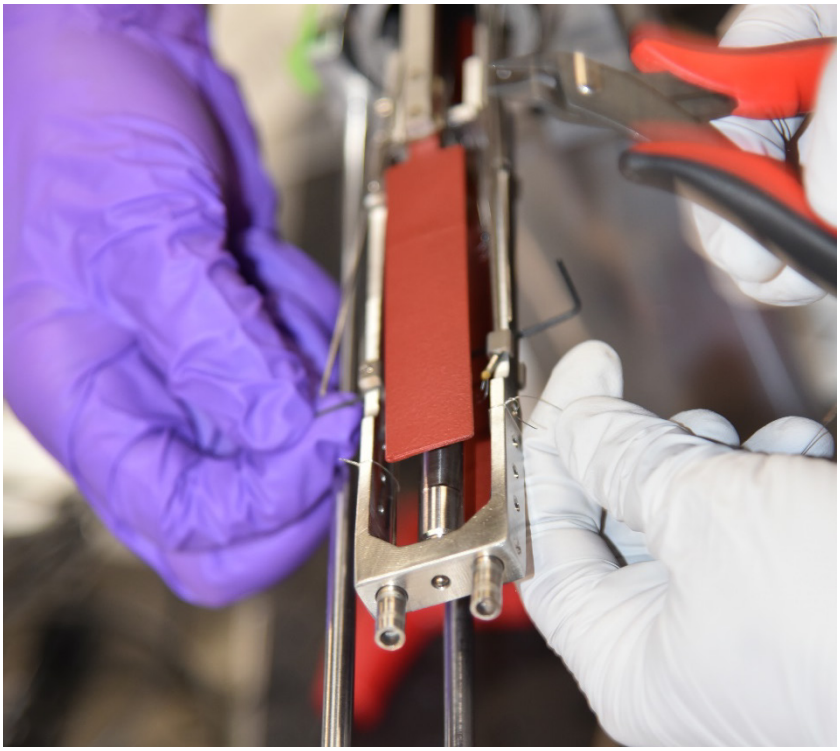

Figure 7. HERA capsule during the assembly process. Two of the fiber optic pressure sensors are seen at the bottom of the image.

The preliminary data from the pressure sensor in the HERA capsule are provided in Figure 8. As was previously mentioned, there is no reference pressure sensor in this capsule, thus nothing against which to compare the data. One strong conclusion that was drawn was that the general behavioral trends resembled what were expected by the principle investigators. Additionally, sufficient signal was achieved throughout the irradiation, with no signs of catastrophic failure. To date, all other pressure sensors tested in the Transient Reactor Test Facility have experienced catastrophic failure (no signal, or outputs the sensor's maximum or minimum pressure limit) after the transient. While more development is necessary to qualify the in-pile performance of this sensor, the present work provides a good foundation for future work to build upon. It is also encouraging that the development path reflects a reasonable trajectory for producing a useful sensor that meets the needs of the nuclear energy community.

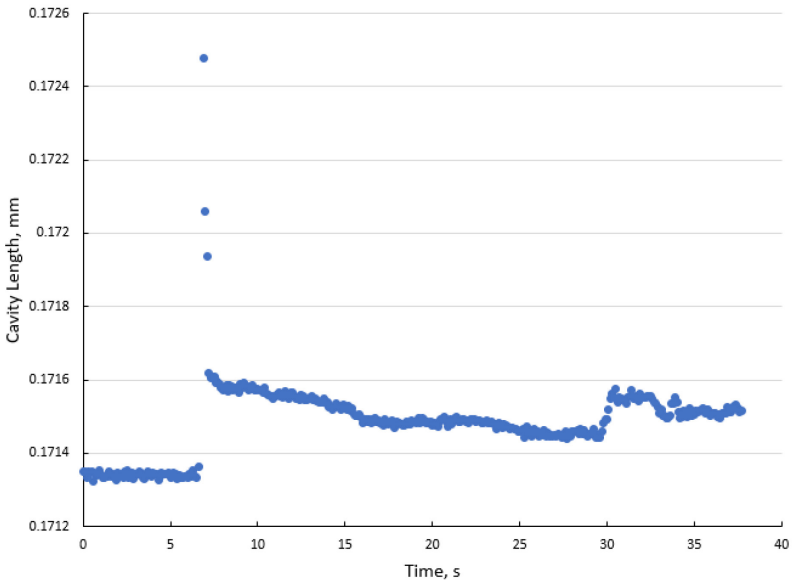

Figure 8. Preliminary results from the pressure sensor used for the HERA calibration transient.

4. SUMMARY AND CONCLUSION

This report documents the motivation, methodology, and progress of developing a fiber-optic-based pressure sensor for nuclear energy applications. The authors recognize that, though they attempted to design this sensor to meet many application requirements, not all such requirements were met (nor is it possible for a single sensor to do so). Therefore, rather than describe a specific sensor configuration, this paper presented a detailed discussion on key components of the sensor, why they were selected, and what the resulting tradeoffs were. This establishes a basis for future work to build upon when sensor modifications are required, and provides future researchers some guidance on how to proceed without repeating significant work.

Reliable—but constantly improving—fabrication and robust calibration processes have been established, and these supported the laboratory-based testing of this novel instrument, as well as provided a foundation for initiating in-pile testing of the sensor. Excellent agreement is observed between predicted sensor performance and experimental results. This indicates the as-built configuration of the sensor closely matches the design intentions. This is valuable because it can enable a reliable methodology to compensation for temperature effects on sensor performance. This in-pile testing kicked off with the HERA irradiation experiment series. While no reference pressure sensor exits for this experiment to compare against, there is still significant value in qualitatively evaluating the sensor performance and identifying challenges. All data presented herein were collected from the first sensor in this experiment series.

5. REFERENCES

1. A. Fleming, J. Daw, J. Smith, P. Calderoni, Research plan for the development of optical fiber pressure sensors for nuclear applications, INL/EXT 18-45711
2. A. Fleming, A. Lambson, Development and Testing of a Fiber-Optic Based Extrinsic Fabry-Perot Pressure Sensor for In-Pile Applications, 2020, INL/EXT 20-00594
3. ASME Boiler & Pressure Vessel Code, 2021